Silicon (2022) 14:1831–1849
https://doi.org/10.1007/s12633-021-01243-9

ORIGINAL PAPER

A Study of Added SiC Powder in Kerosene for the Blind Square Hole Machining of CFRP Using Electrical Discharge Machining

PV Arul Kumar[1] · J. Vivek[2] · N. Senniangiri[3] · S. Nagarajan[4] · K. Chandrasekaran[5]

Received: 26 March 2021 / Accepted: 28 June 2021 / Published online: 9 July 2021

Abstract

Carbon Fiber Reinforced Polymers (CFRPs) have been applied potentially for various application components owing to their lightweight and better mechanical properties. However, the machining of CFRP has been observed to be poor machinability due to the properties of the CFRP composites. Micro-feature fabricating on CFRP macro-component is a challenging task due to the selection of inadequate process parameters and machines. However, micron-level blind square holes are required in CFRPs for proposing the applications of micro-robotics, micro-vibration measurements, and micro-detection of cracking. These square holes produced on CFRP have the difficult task of being machined using the Electrical Discharge Machining (EDM) process. In this research, the effects of concentration of silicon carbide, pulse duration, duty cycle, and current on squareness, hole depth, and surface roughness of CFRPs are analyzed using Electrical Discharge Machining (EDM) with the square copper electrode. The input parameters, the various percentage of concentration of silicon carbide, pulse duration, duty cycle, and current for EDM are selected. The responses, squareness, hole depth, and surface roughness are considered. Also, an electrode wear length and surface defects have been analyzed. The modeling has been performed for selected responses. Additive Ratio Assessment (ARAS) is used for obtaining optimum parameters. The overall analysis found that the silicon carbide concentration and pulse duration are greatly affected all the responses. Also, the square electrodes produced unstable spark phenomena in the EDM process.

Keywords CFRP · EDM · Silicon carbide · Squareness · Depth

1 Introduction

Carbon Fiber Reinforced Polymers (CFRPs) are used in aerospace, satellite, electronic field, and commercial parts. The reasons for using these CFRPs are low density, high strength, low friction coefficient, high toughness, and good wear resistance. Square holes are required in CFRPs for proposing the applications of micro-robotics, micro-vibration measurements, micro-detection of cracks, micron-level relative humidity measurements, micron-level - thermal strain measurements, micro - level -temperature measurements, detection of micro - delamination, and micro-fiber optics. Thereby, the square holes were fabricated on CFRP by using EDM [1–3], laser machining [4], mechanical drilling [5, 6], and micro-EDM [7]. Also, the square hole is mostly used in the precision manufacturing sector for manufacturing the micron-level square in the 3D micro-components for microfluid transportation purposes and

✉ PV Arul Kumar
arulkumarveera@gmail.com

J. Vivek
vivekdynamech18@gmail.com

N. Senniangiri
senniangirinatarajan1987@gmail.com

S. Nagarajan
arsnagarajan@gmail.com

K. Chandrasekaran
kchandrusekaran1984@gmail.com

[1] Department of Mechanical Engineering, Bharath Niketan Engineering College, Aundipatty, Tamil Nadu 625536, India

[2] Department of Mechanical Engineering, Solamalai College of Engineering, Madurai, Tamil Nadu 625020, India

[3] Department of Mechanical Engineering, Nandha Engineering College, Erode, Tamil Nadu 628052, India

[4] Department of Mechanical Engineering, College of Engineering and Technology, Mettu University, Post Box. No 318, Mettu, Ethiopia

[5] Department of Mechanical Engineering, MAM School of Engineering, Trichy, Tamil Nadu 621105, India

increasing the heat transfer rate with acceptable dimensional accuracy. Among the various machining processes, the non-contact and stress-free machining process for EDM is selected to perform machining on CFRP. The performance measures of CFRPs are highly associated with many factors such as electrode materials (copper, graphite, tungsten carbide, etc.,), electrode dimensions (micron and micron size), polarity, types of dielectric mediums (kerosene, EDM oil, distilled water, etc.,) and additives in dielectric mediums (SiC, Si, Cu, etc.,) and selection of process parameters (pulse duration, pulse interval, etc.,). The selection of electrode materials is an important task for obtaining better performance measures. Hence, tungsten carbide electrodes were fabricated by using a wire electric discharge grinding. The 0.110 mm diameter-fabricated electrodes were used for providing the holes on CFRP by using EDM and a 1.2 mm depth of cut was achieved [8]. In another work, 0.5 mm diameter copper electrodes were fabricated for providing blind holes on CFRP by using EDM and 0.25 mm depth of cut was achieved [9]. To evaluate the different electrode material performance over the CFRP machining, copper and graphite electrodes were used on CFRP by using EDM. The results found that copper electrodes gave better performance than graphite electrodes based on the electrode wear and surface finish [10]. Using copper electrodes for making blind holes on CFRC was performed using 1.5 amp current and 200 μs pulse duration and 5.14 μm surface roughness was achieved [11]. The copper electrode wear rate was analyzed for drilling on CFRP by using 1 amp current and 150 μs pulse duration and 0.0056 mg/min electrode wear rate was observed [12]. To reduce the burr formation of CFRP drilled holes, the copper, brass, and aluminum electrodes were selected for drilling on CFRP by using EDM. The results found that the copper electrode gave better results than other electrodes [13]. In another work, burr formation was also reduced using EDM with different electrodes such as aluminum, brass, steel, and copper were selected for processing on CFRP. The results found that the copper electrode produced better results than other electrodes [14]. Besides, the selection of EDM parameters is also important to improve performance measures. The current was directly proportional to the tool wear rate by EDM drilling on CFRP [15]. Hence, the low electrode wear was observed by lowering the current. The 5 amp current and 100 μs pulse duration were used to obtain the 4.8 μm surface roughness of CFRP. The results found that the current was increased with an increase in the surface roughness. Hence, the low current is recommended for obtaining low surface roughness and less thermal damages [16]. The approximately 4 μm surface roughness was obtained using a pulse duration of 70 μs and a current of 2 amp in EDM drilling [17]. The Powder-Mixed Electric Discharge Machining (PMEDM) is also used for improving the performance measures. The dielectric medium has also played an important role in improving machining characteristics by alternating ionization, heat dissipation, and dielectric flushing. Besides, dielectric medium physical parameters such as breakdown strength, flash point, thermal conductivity, pressure, flushing velocity, density, and viscosity influence the performance of EDM. Hence, these properties are directly associated with the selection of hydrocarbon dielectric fluid, water-based dielectric fluid, and gas-based dielectric fluid. The special technological behaviors of hydrocarbon dielectric fluids are small tool wear, high metal removal, and no corrosion of sample, low flash point, and no deionization necessary. Therefore, the hydrocarbon dielectric fluid of kerosene has been selected as a dielectric medium for obtaining more stable and effective machining performance than another dielectric medium [18]. Also, the dielectric medium performances are improved by adding different types of additives such as carbon, aluminum, copper, nickel, silicon, graphite, tungsten, and titanium powder [19]. Among the various additives, SiC powder is selected as an additive because of its superior properties. Hence, the effects of PMEDM process parameters on squareness, hole depth, and surface roughness of CFRPs are focused on it. The reasons for selecting the PMEDM are enlargement of the discharge gap, widening of discharge passage, multiple discharges, and influences of powder properties on machining characteristics. The surface roughness was reduced by increasing the concentration of SiC powder added to EDM oil [20]. Similarly, the material removal depth was decreased by increasing the concentration of SiC powder added to pure water [21]. SiC powder ranging from 5 g/l to 20 g/l was added to deionized water for improving the surface roughness. The result found that the 25 μs pulse duration produced the 6.77 μm surface roughness and it was a higher surface roughness value compared to 50 μs pulse duration due to the uneven distribution of discharges [22]. The material removal depth and surface roughness were analyzed by adding Al to kerosene and SiC to kerosene and kerosene. The result identified the addition of Al/SiC to kerosene-improved performance measures compared to kerosene [23]. Kerosene is one of the main dielectric fluid mediums for machining micro-hole on steel and produces effective machining on steel using EDM. The results found that the entrance diameter was greater than the exit diameter and the tungsten carbide electrode wear was 273 μm obtained [24]. The hybrid machining processes were also used to fabricate the micro-holes of diameter 250 μm on steel using micro-EDM with 100 V voltage and 1500 pF capacitance [25]. The electrode diameter greatly affected the MRR, TWR, and taper angle. Increasing in the MRR, TWR, and taper angle were observed by increasing the electrode diameter [26]. Micro-hole comparative studies were made between the laser and micro-EDM on nickel-based superalloy by using selected optimum process parameters. The results found that micro-EDM has

produced better hole geometry than laser processes [27]. In another strategy, the 0.32 μm surface roughness of AA-10%SiCp MMC was achieved by using powder concentration 4 g/L, pulse duration 100 ms, current 3 A, and voltage 50 V [28]. Comparative surface roughness was studied between the aluminum powder and silicon powder in the machining of EDM by using selected working conditions. The results found that 2 mm surface roughness was obtained and an aluminum powder gave a greater influence on surface roughness than silicon powder [29]. The performance of PMEDM and Rotary-EDM were studied based on the material removal rate (MRR) and tool wear rate (TWR). The results identified that the PMEDM process gave better performance than die-sinking EDM [30]. The EDM process can also be used for removing the burr from the machined CFRP due to the spark energy. The results found that oxygen showed higher MRR than negative polarity. Moreover, EDM oil gave a more effective performance for unwanted burrs removal from the EDM [31]. The coated carbide drill was used for machining of CFRP based on the tool life and hole quality CFRP/titanium stack. The output of the result found that the CFRP/titanium stack produced poorer quality than the individual machining of material [32]. The performance nano-powder of Fe2O3 over the Co-Cr-Mo sample was studied by using micro-EDM. The results identified that material depth was significantly improved by adding 2 g/l of nanopowder in the dielectric medium [33]. To reduce the machining time, the morphology of the machined surface, and deviation in channel width, the assisting-electrode method was used for creating micro-channels (depth: 400 μm and length: 3000 μm) on CFRP using brass and copper of 960 μm in diameter. The SEM results found that peripheral surface damage, spalling, fiber breakage, and debris accumulation were observed [34]. Influencing in the cut direction and process parameters on depth of cut and surface roughness were studied and found that a 16% increasing in the material removal rate was observed when machining parallel to fiber direction compared to cutting perpendicular to the fibers, which was attributed to the higher electrical conductivity of the workpiece along the fiber length leading to greater discharge energies [35]. The low-frequency vibration-assisted EDM on CFRP was also used for improving machining efficiency and stability [36].The shape of electrode and assisting-electrode were used for improving the micro-electrical-discharge drilling performance of CFRP resulting in the voltage was a significant factor that affecting the performance measures [37]. The influence of a short circuit on machined surface quality CFRP was investigated using EDM and found that the machining was stopped when the EDM in an unstable state due to the short circuit [38]. To increasing the material removal rate of CFRP and reducing in tool wear, carbon black and graphite (fillers) were added to the matrix for increasing the electrical and thermal conductivity and the result found that high machinability, low thermal damage, and good surface quality were observed [39]. The μEDM integrated with a rotary tool and assisting-electrode was used for efficient spark generation in EDM. The result found that the material removal mechanism was a complex phenomenon where sparking happened both at the side surface and end face of the tool [40]. The effect of EDM process parameters such as feed rate and voltage on the hole quality was studied by micro-EDM and found that the microhole of 2500 μm deep was achieved in CFRP [41]. The sandwich assisting-electrode method was used for cutting off thin CFRP and found that matrix cracking, breakage of carbon fibers, and fiber-matrix debonding were observed [42]. The preheating method was used for machining CFRP and found that very small, thin, and deep microfeature creating on CFRP was observed for enhancing their micro-features performance and function [43]. The previous studies found that the addition of powder particles in the dielectric medium effects on MMCs have also been used for improving the process performance of different work materials [44–49]. The optimization tools such as Taguchi's method, support vector machine, artificial neural network, and response surface methodology have also been used for improving the performance measures of polymer-based composites [50–52].

Few works have been found that effects of micron-level square shape electrodes with EDM process parameters and various percentages of SiC powder-mixed in the kerosene medium effects on squareness, hole depth, and surface roughness of CFRPs have been studied. More works have focused on macron-level circular hole profile processing on CFRP using EDM. Hence, the blind square holes in CFRPs have been focused on using the EDM parameters with a concentration of SiC powder. The CFRP application component requires blind-square holes during their usage. But, the blind square holes produced on CFRP have a difficult task by using electrical discharge machining process parameters with micron-level copper electrodes due to the variations in the material properties of carbon fiber and epoxy resin. Moreover, blind holes produced on CFRP are a challenging task due to the low melting point of copper electrodes produced by high electrode wear in the micro-scale machining of CFRP. Therefore, the machinability of CFRP has been analyzed on the basis that the squareness, hole depth, and surface roughness are focused on it. The micron-level square blind holes fabricating on CFRPs are the primary task. Hence, squareness and hole depth are important geometrical features for affecting the functionality of the relative motion between the machined parts. Therefore, these responses are mainly focused on it. The most contributing factor is identified by analysis of variance. Additive Ratio Assessment (ARAS) is used for obtaining optimum parameters. The electrode wear and surface defects are also analyzed. Finally, a comparative

analysis is carried out between a present study and previous results.

2 Material and Methods

2.1 Fabrication of CFRP

The autoclave process is normally used for producing CFRP laminates and this process is carried out under a pressurized vessel for applying pressure and heat to both parts that have been sealed in a vacuum bag. A prepreg carbon fiber-epoxy material is laid out on a work table to ensure that fiber orientation meets the design requirement, where the prepreg material consists of unidirectional long-carbon fibers in a partially cured epoxy matrix. The pieces of the prepreg material are cut out and placed on top of each other on a shaped tool to form a laminate. The layers could be placed in different directions to produce the desired strength pattern since the highest strength of each layer is in the direction parallel to the fibers. After the required number of layers has been properly placed, the tooling and the attached laminate are vacua bagged, for removing the entrapped air from the laminated part. Finally, the vacuum bag and the tooling are put into an autoclave for the final curing of the epoxy resin. After removal from the autoclave method, the composite material is ready for further finishing operations.

2.2 Micro-Drilling

The micro-holes in the form of square shapes were performed on CFRP, a problematic task owing to their properties of composites. Table 1 shows the properties of SiC, kerosene, copper electrode, carbon fiber, and epoxy resin. Specification of EDM drill is shown in Table 2.Table 3 shows the selection of EDM process parameters and difficulties faced by selecting the EDM process parameters. Therefore, the blind square hole was performed on CFRP using EDM. These square holes produced on CFRP were a difficult task of being machined using the Electrical Discharge Machining (EDM) process due to the need for selection of proper parameters, its associated performance measures, and variations in the CFRP material properties. Electrical Discharge Machining (EDM) has been used to machine difficult to cut material and the process is not related to the hardness of the material. The EDM and Abrasive Jet Machining (AJM) processes have also been used for machining CFRP. Moreover, the strength of CFRP is reduced after AJM processing due to the more water-absorbing properties of CFRP [53]. The usage of abrasive water jets for machining CFRP is not considered due to the delamination, burr, fiber pull-out, poor geometrical shape, dimension accuracy, and kerf width reduction [43], the more striation formation on the machined surface [54], abrasive grain size greatly affected the surface roughness [55], approximately the surface roughness varying from 3 to 4 μm [56, 57], low penetration depth [58]. Hence, compared to previous works [54–58], the abrasive water jet machine is producing lower performance measures compared to the EDM process [7, 10, 11, 16, 22]. Therefore, EDM is selected for processing on CFRP. The kerosene dielectric pressure was 0.7 kg/cm^2 fixed as constant. According to the design of the experiment, the blind square holes were performed on CFRP for studying the effects of the parameters on squareness (Sq. ness), hole depth (HD), and Surface Roughness (SR). The schematic line diagram and photocopy of EDM are shown in Fig. 1.

Table 2 Technical specification of EDM drill

Machine tool	value
Work table	400×400
Max electrode length	400 mm
Size of electrode diameter	0.3 to 3.0 mm
Maximum drill depth	250 mm
Maximum coolant pressure	60 kg/cm^2
Maximum weight of work piece	300 kg
Work tank	690×470×83 mm
Net weight	750 kg
Connected load	2 KVA
Input power supply	3 phase, AC 415 V, 50 Hz
Maximum machining current	20 amp

Table 1 Properties of SiC, kerosene, copper electrode, carbon fiber and epoxy resin

Material	Specific heat (J/kg K)	Breakdown Strength (kV/mm)	Density (g/cm^3)	Electrical Resistivity (μΩ cm)	Flash point (°C)	Melting Point (°C)	Thermal Conductivity (W/mK)
Silicon carbide (SiC)	510–650	–	3.22	1013	–	2730	300
Kerosene	2100	24	0.81	–	37–65		0.14
Copper	0.39	–	8.93	0.009–0.07 μΩ × 10^{-4}		1083	401
Carbon fiber	2020 at 1230 °C	–	2.267	–	–	3652–3697	0.17–0.79
Epoxy resin	1110 J/kg °C	–	1.1–1.4	–	–	140	0.2

Table 3 Selection of process parameters

Parameters	Units/ Symbol	Levels				Machine limits/ From the literature papers/ Problems observed
		1	2	3	4	
Concentration of SiC	g/l / Cp	4	8	12	16	[59, 60]
Pulse duration	μs / Ton	15	30	45	60	Machine limit
Duty cycle	% / DC	1	3	5	7	Slow material removal rate
Current	amp/ I	2	4	6	8	Higher electrode wear observed by rising above 8 amp

Figure 2 shows the EDAX for CFRP composites and found that the chemical compositions of CFRPs identified by EDX are 84.12%C, 0.20%Si, 14.92%O, 0.28%CI, 0.20%Na, 0.21%Ca and 0.10%K. The responses such as Concentration of SiC (g/l), Pulse duration (μs), Duty cycle (%), and Current (amp) were taken as EDM inputs. To achieve the blind square holes on CFRPs, the square copper electrodes were prepared using a vertical machining center and the sample copper electrode is shown in Fig. 3. The fresh copper electrode dimensions were measured using a coordinate measuring machine. The mean widths and standard deviations for 0.8 mm square electrodes were in the dimension of 0.8018 ± 0.017 mm. The hole depth, major axis, and minor axis of the blind hole parameter are shown in Figs. 4 (a-b). The scanning electron microscope (ZEISS: Coordinate Measuring Machines), video-measuring system (VMS-2010 F) were used for measuring the squareness, hole depth, and surface roughness. The top surface of blind square hole squareness is calculated using Eq. 1. The squareness value ranges from zero to one. Squareness value is one denoted as a perfect square. The electrode wear length can be measured along with the height of the electrode by taking the difference between the fresh electrode lengths to worn out electrode length and surface roughness were measured using SURFCOM TOUCH 50 tester.

$$Squareness\ (sq.ness) = \frac{Major\ axis}{Minor\ axis} \tag{1}$$

2.3 Additive Ratio Assessment (ARAS)

The additive ratio assessment is a multi-criteria decision-making method [61]. The method is presented in the tabular form and not in matrix form for a better understanding of the mechanism. ARAS selects the best alternative based on many attributes and the final ranking of alternatives is made by determining the utility degree of each alternative. ARAS has one of the compensatory methods, and qualitative attributes are converted into quantitative attributes and attributes are independent. The steps are given below.

Step 1: Forming of Decision-making matrix (DMM).

The under-mentioned DMM of preferences (Xij) for 'm' alternatives (rows) rated on 'n' criteria (columns):

$$X = \begin{bmatrix} x_{01} & x_{01} & \cdots & x_{0n} \\ x_{11} & x_{12} & \cdots & x_{1n} \\ \vdots & \vdots & \vdots & \vdots \\ \vdots & \vdots & \vdots & \vdots \\ \vdots & \vdots & \vdots & \vdots \\ x_{m1} & x_{n2} & \cdots & x_{mn} \end{bmatrix} \tag{2}$$

Where i = 0,1,…,m; j = 1,2,….,n.

Xij is the value corresponding to the performance value of the alternative named i, under the j criterion while xoj is the optimal value for the j criterion. When the optimal value of the j criterion is absent, then

$$X_{oj} = \left\{ \begin{matrix} \max x_{ij}\ if\ J \in B \\ \min x_{ij}\ if\ J \in C \end{matrix} \right\} \tag{3}$$

Here, B and C are denoted the benefit criteria to be maximized and non-benefit criteria to be minimized, respectively.

Step 2: Normalization of decision-marking matrix.

Linear normalization methodology is used to different criteria.

$$\overline{x}_{ij} = \frac{x_{ij}}{\sum_{i=0}^{m} x_{ij}} \tag{4}$$

The minimum criteria are normalized through a two-stage process.

$$x_{ij} = \frac{1}{x_{ij}^{*}}; \overline{x}_{ij} = \frac{x_{ij}}{\sum_{i=0}^{m} x_{ij}} \tag{5}$$

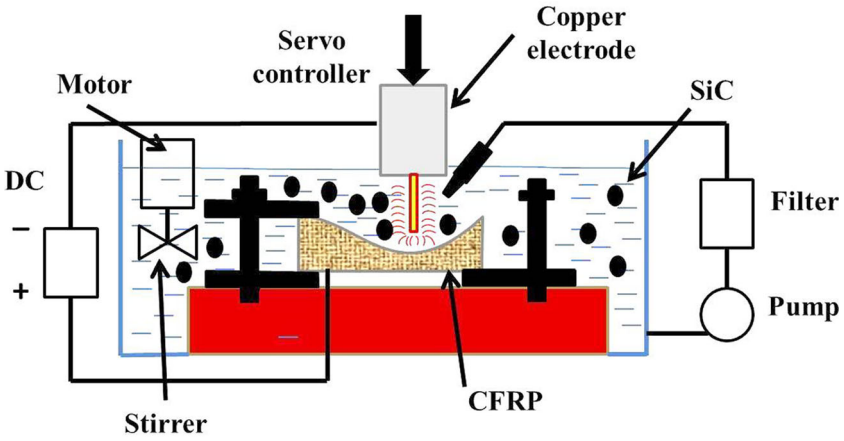

(a)

(b)

Fig. 1 EDM: (a) Schematic diagram, (b) photocopy of EDM

Step 3: Weighted normalized decision matrix

$$\widehat{X}_{ij} = \overline{x}_{ij} * w_j; \quad i = 0, \ldots, m, \tag{6}$$

$$\widehat{X} = \begin{bmatrix} \widehat{x}_{01} & \widehat{x}_{01} & \cdots & \widehat{x}_{0n} \\ \widehat{x}_{11} & \widehat{x}_{12} & \ldots & \widehat{x}_{1n} \\ \vdots & \vdots & \vdots & \vdots \\ \vdots & \vdots & \vdots & \vdots \\ \vdots & \vdots & \vdots & \vdots \\ \widehat{x}_{m1} & \widehat{x}_{n2} & \ldots & \widehat{x}_{mn} \end{bmatrix} \tag{7}$$

Where, i = 0,1,…,m; j = 1,2,….,n.

$\widehat{X}_{ij}$ is the weighted normalized performance rating of the i alternative through the j criterion.

Step 4: Determine the optimality function (Si) for the alternative

$$Si = \sum_{j=1}^{n} \widehat{x}_{ij} \tag{8}$$

Where, i = 0,1,…,m; j = 1,2,….,n. and High Si value is better alternative.

Step 5: Determine the degree of utility (Ki) for each alternative.

$$K_i = \frac{S_i}{S_o}; i = 0, 1, \ldots, m \tag{9}$$

Step 6: Rank the alternatives based on Ki values.

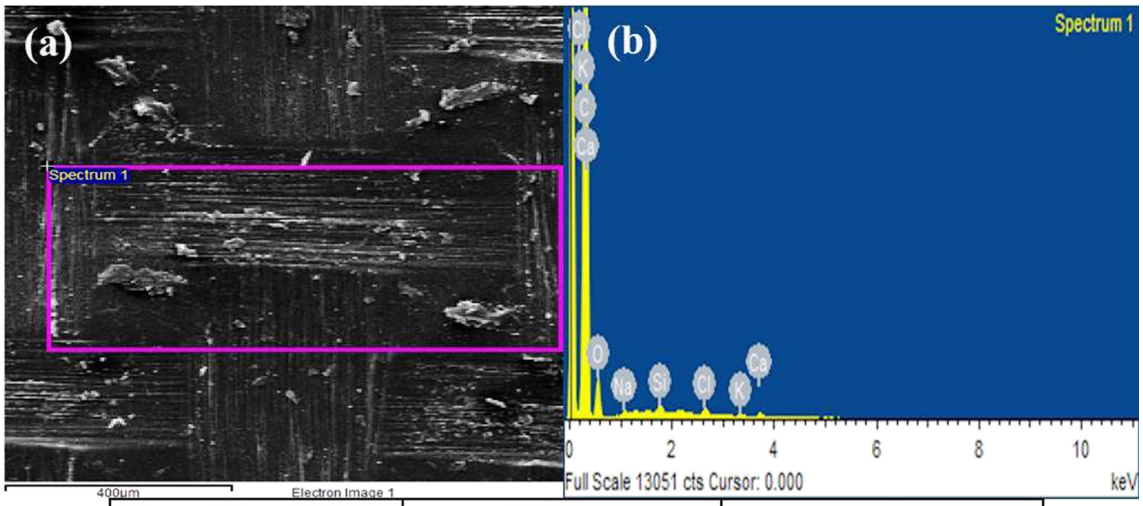

(C)

Element	Weight%	Atomic%
C K	84.12	87.92
O K	14.90	11.69
Na K	0.20	0.11
Si K	0.20	0.09
Cl K	0.28	0.10
K K	0.10	0.03
Ca K	0.21	0.06
Totals	100.00	

Fig. 2 EDAX for CFRP

3 Results and Discussions

The primary purpose of the work is to fabricate a blind square hole on CFRP using EDM process parameters. Also, the effects of the addition of SiC particles in the kerosene fluid on squareness, hole depth, and surface roughness of CFRPs are studied. The analysis of blind square hole feature studies is an important task. This is because the selected responses greatly affected productivity and production. The responses such as squareness, hole depth, and surface roughness are considered. The blind square hole tests are carried out on CFRP as per the design of the experiment. The responses are measured and recorded. Table 4 shows the design layout and result of squareness, hole depth, and surface roughness of CFRP. Table 5 shows the calculation of the mean response.

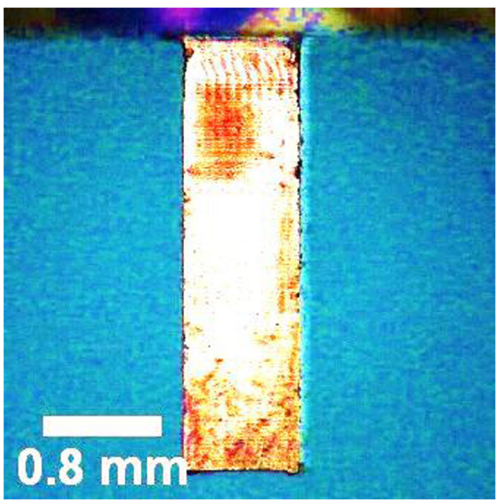

Fig. 3 Optical microscope image of copper electrode

3.1 Squareness

Experimental results found that the squareness value was greater than one in the entire square hole. This was due to the major axis being higher than the minor axis. Variations in the thermal properties of carbon fiber, epoxy resin, and SiC particles were also reasoned for obtaining a squareness value greater than one. The direction of the dielectric kerosene flushing, pressure, and concentration of SiC was also a reason for varying the square hole size in the experimental results. The unstable spark generated from the non-circular electrodes and corner radiuses of micro-feature formed on the work materials were observed. The previous works found that the non-circular electrode shapes were produced the unstable spark to Inconel 718 and Inconel 625 [62, 63]. In another way, to enhance the thermal properties of the dielectric medium strength, the addition of SiC concentration to kerosene was carried out and it was proved that the addition of SiC

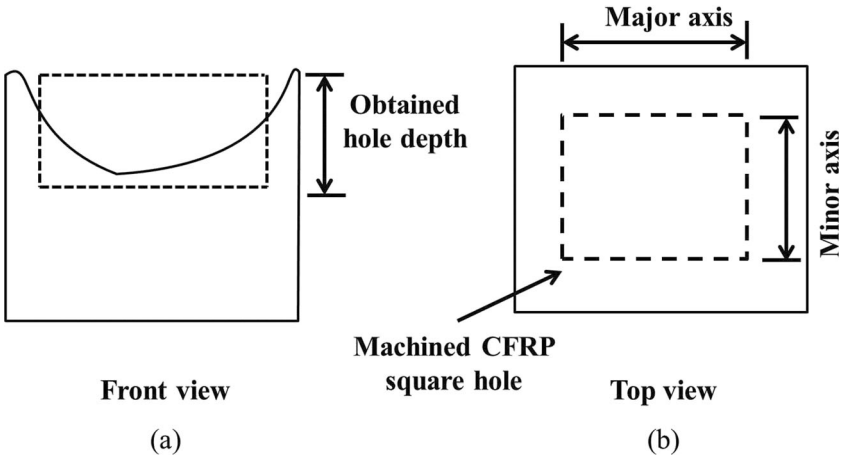

Fig. 4 Schematic diagram for blind square hole: (a) hole depth, (b) major axis and minor axis

concentration to kerosene was greatly affected dielectric medium-strength [44]. Hence, the addition of SiC concentration to kerosene was carried out. After drilling, the graphs were drawn between the process parameters and responses. On increasing the concentration of SiC and pulse duration, the squareness increased and it is shown in Fig. 5. The squareness variations of micro-holes were due to the differences in the melting point of carbon fiber and epoxy resin. Also, epoxy resin has a lesser melting point compared to carbon fiber. Variations in the thermal conductivity and melting points were observed between the carbon fiber and epoxy resins that also reasoned for variation in the squareness of micro-holes. Moreover, the square shape copper electrode was generated non-uniform high-density sparks to CFRPs, resulting in increasing squareness. More electrothermal energy was used for melting and vaporizing the CFRP. In addition, the direction of kerosene-flushing pressure was also intended for increasing the squareness. Therefore, squareness increased. With an increase in the duty cycle, the squareness decreased. The eroded materials were difficult to remove away from the machined zone by increasing the viscosity of the dielectric medium. Also, decreasing in the squareness was due to the effect of SiC powder particles on CFRP, surface properties, particle size, and electrostatic forces. Therefore, the squareness decreased. On increasing the current, the squareness decreased up to the level of 4 amp current and then rose above 4 amp current. This was due to the unstable spark generated from the square electrode to CFRP. The debris accumulation

Table 4 Design and experimental results

Exp. No.	Input process parameters				Quality performances		
	Concentration of SiC (g/l)	Pulse duration (μs)	Duty cycle (%)	Current (amp)	Squareness –	Hole depth (mm)	Surface roughness (μm)
1	4	15	1	2	1.044	0.177	1.941
2	4	30	3	4	1.067	0.180	2.565
3	4	45	5	6	1.120	0.181	3.623
4	4	60	7	8	1.132	0.197	3.652
5	8	15	3	6	1.026	0.222	3.691
6	8	30	1	8	1.076	0.255	4.254
7	8	45	7	2	1.121	0.297	4.656
8	8	60	5	4	1.135	0.322	4.752
9	12	15	5	8	1.049	0.342	4.796
10	12	30	7	6	1.089	0.370	5.044
11	12	45	1	4	1.145	0.394	5.374
12	12	60	3	2	1.158	0.405	5.836
13	16	15	7	4	1.031	0.409	5.846
14	16	30	5	2	1.099	0.446	6.005
15	16	45	3	8	1.147	0.466	6.094
16	16	60	1	6	1.161	0.505	6.527

Table 5 Mean responses calculation

Levels	Cp	Ton	DC	I
Squareness				
1	1.091	1.038	1.107	1.105
2	1.090	1.083	1.099	1.095
3	1.110	1.133	1.101	1.099
4	1.109	1.147	1.093	1.101
Maximum	1.110	1.147	1.107	1.105
Minimum	1.090	1.038	1.093	1.095
Delta	0.020	0.109	0.013	0.011
Rank	2	1	3	4
Improvement percentage (IP)	1.84	9.51	1.18	0.99
Hole depth				
1	0.184	0.287	0.333	0.331
2	0.274	0.313	0.318	0.326
3	0.378	0.335	0.323	0.320
4	0.457	0.357	0.318	0.315
Maximum	0.457	0.357	0.333	0.331
Minimum	0.184	0.287	0.318	0.315
Delta	0.273	0.070	0.014	0.016
Rank	1	2	4	3
IP	59.79	19.51	4.33	4.95
Surface roughness				
1	2.945	4.068	4.524	4.609
2	4.338	4.467	4.546	4.634
3	5.263	4.936	4.794	4.721
4	6.118	5.192	4.799	4.699
Maximum	6.118	5.192	4.799	4.721
Minimum	2.945	4.068	4.524	4.609
Delta	3.173	1.123	0.276	0.112
Rank	1	2	3	4
IP	51.86	21.64	5.74	2.36

in the machined zone was also reasoned for variations in the squareness. Hence, the applied current showed that the steep V-shaped change in the behavior of squareness. In Table 5, it was found that the pulse duration was the most significant factor that affects the squareness of blind square holes. Improvement in the squareness percentages was calculated based on the parameters to rate the different machining performances. The pulse duration was used for obtaining a maximum improvement in the 9.51% squareness. Thereby, the minimum squareness was obtained using the 8 g/l concentration of SiC, 15 μs pulse duration, 7% duty cycle, and 4 amp current. Also, the duty cycle and current were used for improving the squareness at a low level. Previous results identified that the metal removal rate of CFRP was increased using 500 μs pulse duration [11]. Here, metal removal rate and squareness behavior were similar owing to both responses related to geometric features. Hence, lowering the pulse duration was used for obtaining minimum squareness. In another study, the thermal conductivity of the dielectric medium was increased by increasing the concentration of graphite to dielectric fluid for improving the material removal rate [24]. Similar results were also obtained in this work. The unstable sparks generated from EDM electrodes were affecting the process performances. The direction of dielectric fluid flushing was also greatly affecting the machined surface [64].

3.2 Hole Depth

The hole depth (machined depth) varied by increasing the process parameters and it is shown in Fig. 6. It was found that the concentration of SiC and pulse duration were the most influenced factors on hole depth. The 16 g/l concentration of SiC and 60 μs pulse duration were used for obtaining the maximum hole depth on CFRP. This was due to the higher thermal energy generated from the SiC mixed dielectric fluid to the machining region. SiC powder mixed with kerosene has provided stable machining by increasing the thermal conductivity of the dielectric fluid. Hence, hole depth increased. Besides, by raising the pulse duration, the hole depth increased owing to the unstable spark with higher thermal energy produced in the square electrode to CFRP. The effects of SiC powders mixed to dielectric fluid; the powder energized and performs in a zigzag movement between the copper electrode and CFRP. Effects of zigzag movement of particles formed the chain structure in the machining zone and reduce the dielectric fluid strength and develop a series discharge. The result found that the electrode sparking area produced effective discharge transmissivity owing to the raises in thermal conductivity. Therefore, the hole depth increased. Raising in the duty cycle and current, and the hole depth decreased. The hole depth variations in the micro-holes due to the differences in the melting point of carbon fiber and epoxy resin. Also, epoxy resin has a lesser melting point compared to carbon fiber. Variations in the thermal conductivity were also observed between the carbon fiber and epoxy resins that also reasoned for variation in the hole depth of micro-holes. Hence, hole depth varied. Normally, the current was directly related to metal removal. Nonetheless, the decrement in the metal removal was due to the eroded materials' difficulty to move away from the machined zone by increasing the viscosity and conductivity of the dielectric medium. More debris and thicken heat-affected zone were formed on the machined zone. The selection of dielectric fluid pressure also greatly affects the electrical properties of dielectric fluid due to the contamination of electrolytes resulting in reducing the efficiency of material removal. In this work, the 0.7 kg/cm^2 kerosene dielectric pressure was selected for processing. It was found that the pressure value was inadequate for removing the debris from the machining zone resulting in debris clogs in the

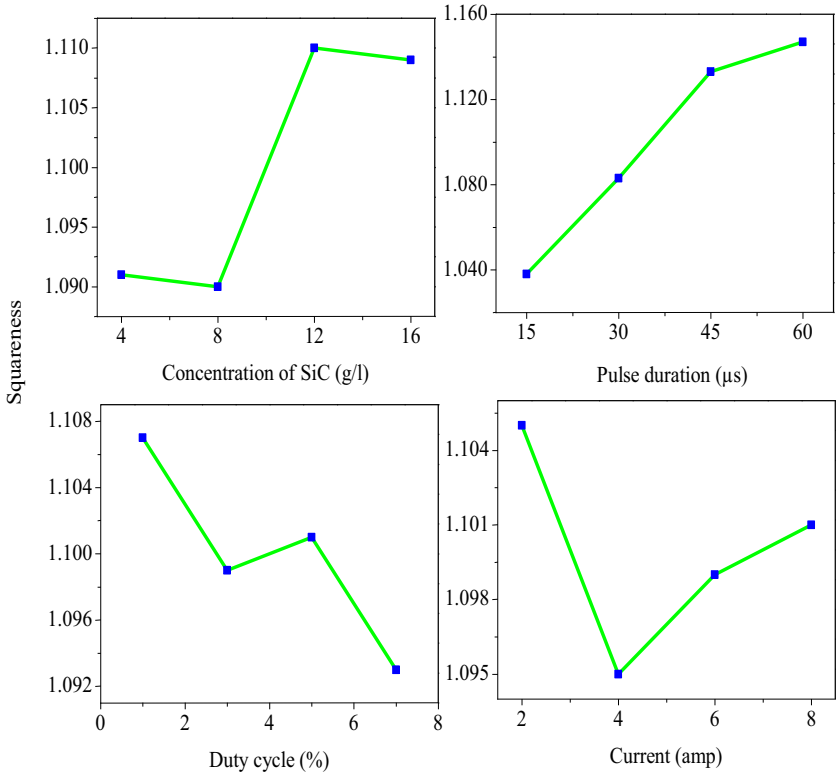

Fig. 5 Effect of parameters on squareness

machining zone. Simultaneously, the spark was supplied continuously without removing work material resulting in a thicken heat affected zone formed. Hence, the hole depth decreased. The 59.79% hole depth was achieved using the 16 g/l SiC concentration. Therefore, the maximum hole depth was obtained using 16 g/l SiC concentration, 60 µs pulse duration, 1% duty cycle, and 2 amp current. The copper electrode wears also affected the width and depth of the hole [25]. Another result found that a higher depth of cut on copper was obtained using a 2.3 amp current and 0.2 µs

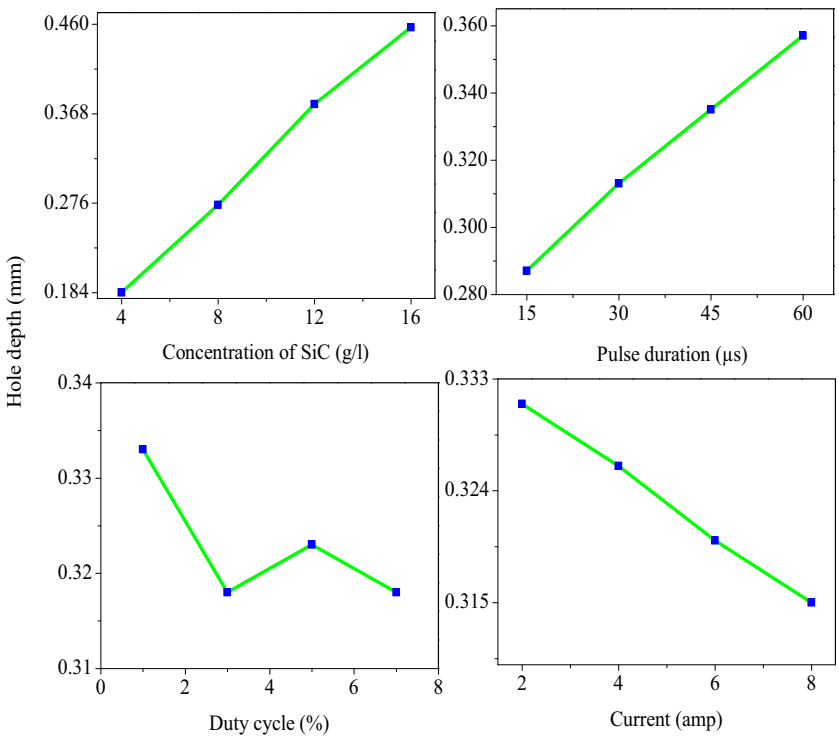

Fig. 6 Effect of parameters on hole depth

pulse duration. The present hole depth agreed well with the previous result [26]. The duty cycle equally affecting the squareness and hole depth due to the nature of CFRP material properties. Hence, the duty cycle produced similar trends over the squareness and hole depth. But, slight variances were also observed between the squareness and hole depth due to the geometrical differences.

3.3 Surface Roughness

Variation in the surface roughness was observed by varying the process parameters and it is shown in Fig. 7. It was found that the concentrations of SiC and pulse duration were the most influencing factors that affecting the surface roughness. The 4 g/l concentration of SiC and 15 μs pulse duration were used for obtaining low surface roughness. The SiC powder mixed dielectric medium destroyed the insulation easily for reducing the electrical resistivity of the medium and leaving the discharge gap resulting in reduce the impulse force of the discharge channel. This influence on the machining gap generated a high plasma channel from a sample to an electrode for increasing the material removal rate. The higher thermal conductivity of copper electrodes was also supported by increasing the material removal rate. Also, carbon fiber and epoxy resin were easily melted, and smoothly surface formed due to the electrothermal effect. Hence, the machined surface showed an uneven small size crater and small debris, resulting in produced low surface roughness. Increasing the surface roughness was observed by raising the SiC concentration, pulse duration, duty cycle, and current. This was due to the increased thermal conductivity and impulsive force in the plasma region. The melting point difference between the carbon fiber and copper electrode was three times higher, resulting in the large and deep crater produced on the machined surface. Hence, higher surface roughness is produced. In short, the low concentration of SiC with low thermal energy sparks produced a lower surface roughness. Thereby, low thermal energy produced small crater sizes in the machined zone. SiC concentration and pulse duration were increased, and surface roughness was increased. The unstable sparks produced deep and wide surface irregularities in the machined zone. Hence, surface roughness increased. Similar behavior was observed in the current and duty cycle. The 51.86% surface roughness was achieved by lowering the SiC concentration. Hence, the minimum surface roughness was obtained using 4 g/l SiC concentration, 15 μs pulse duration, 1% duty cycle, and 2 amp current. The erosion process produced a 10 amp current, which was used to obtain the 1.95 μm surface roughness on titanium [24]. Compared to another study, higher surface roughness was observed in a previous study [27]. This result agreed well with this surface roughness result.

3.4 Electrode Wear Length

Figure 8 shows the copper electrode worn-out surface and worn-out length. After machining, the square form of the copper electrode was transformed into a semi-spherical shape electrode with worn-out length and surface. The main reason for the higher worn-out surface and length was unstable discharge energy produced in the square electrode. Initially, the sharp edge of the copper electrode was worn out and the surface of the electrode was secondly worn out due to the difference in the stress concentration. The copper electrode was a low melting point compared to carbon fiber, epoxy resin, and SiC particles. Hence, the copper electrode was worn out in a short time compared to other materials. Nonetheless, powder mixed dielectric fluid motivated to reduce the worn-out length due to the uniform discharge to sample and increasing the thermal conductivity of the dielectric fluid. Similar behavior was observed in the cylindrical shape electrode due to the skin effect [28]. Hence, electrode wear was an unavoidable problem in spark machining. The work was also focused on reducing the worn-out length of copper electrodes. The electrode worn-out length is reduced by increasing the SiC concentration in the dielectric fluid because SiC powder added to kerosene disturbs the adherence of atoms attached to the electrode surface and reduces the electrode-worn length. Also, SiC powder concentration was equally spread over the dielectric medium and it was nominal electrode-worn length obtained due to better conduction of discharge. The worn-out length of the electrode was varied from 0.31 mm to 1.168 mm by increasing the SiC concentration. The worn-out length was greatly associated with powder properties (concentration, density, thermal conductivity, and electrical resistivity) and it was affecting the machining performance, worn-out surface, and worn-out length. Similar results were observed in previous studies [13, 29]. The heat-affected zone formation and worn-out surface on the copper electrode were also reduced by increasing the SiC powder concentration due to the uniform mixing of powder in the dielectric fluid produces consistent discharge. The small cracks and pores were formed on the copper electrode due to the high impulsive forces developing on the machining zone. The reason for developing high impulsive force was high discharge energy produces more melting and evaporation.

3.5 Surface Defects

In Fig. 9, the corner radius was formed in the machined square hole. The reason for forming a corner radius was the square copper electrode wear. The different melting points of SiC, copper electrode, carbon fiber, matrix resin, and a high degree of short-circuit development were also reasoned. Sharp edges of square copper electrodes were first worn out for generating the round-shaped edges in the machining.

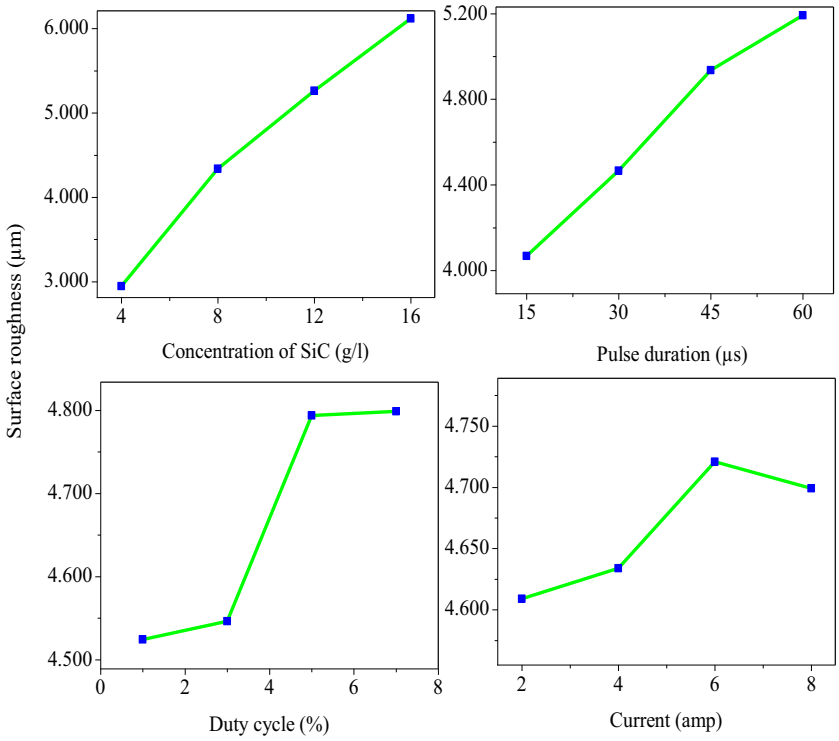

Fig. 7 Effect of parameters on surface roughness

This was due to the difference in the stress concentration factor between the copper electrode and machined hole of the CFRP composite. Simultaneously, the copper electrode wear reflected the sample through sparking. Hence, a corner radius was formed due to the non-uniform spark generated. The burrs were formed on the machined surface due to the long duration of time for developing plasma spark. The copper electrode produced a burr in the machined CFRP using 150 µs pulse duration and it is shown in a previous study [30]. The delamination was also observed due to the longer pulse duration. More heat energy generation at high pulse duration was the reason for generating delamination in the machined CFRP. Moreover, the fibers pulled in/out were observed. A different melting point of carbon fiber and matrix resin was reasoned. A similar result was observed in a previous study [31]. Another study stated that the direction of heat transformed was related to the direction of the carbon fiber orientation and not to the direction of current flow [12]. But, the argument result was observed in this study due to the electrothermal energy developed from the higher pulse duration and current. The heat-affected zone formed around the micro square hole was due to the different thermal conductivity of carbon fiber and epoxy resin. The heat transfer rate of carbon fiber was greater than the epoxy resin due to the higher thermal conductivity of carbon fiber. Due to the poor thermal conductivity of epoxy resin, the problem in heat-transferred rate was observed, affecting the heat-affected zone formation. Similar results were also observed in the previous work [32]. The corner radius was also formed in the machined monel 400 alloy using EDM [65]. This was good supportive work for forming the corner radius formed in the machined surface. More debris and black products were formed in the machined surface of CFRP and the amount of debris formation was highly related to material removal mechanism, selection of the shape of electrode and material, dielectric fluid pressure, EDM process parameters (pulse duration, duty cycle, current) and physical and thermal properties of a powder particle. There were various reasons for forming debris and black portion (thickened heat affected zone formation), which were described below as. By using the low discharge energy in the deep hole machining, debris removal was a challenging issue due to the narrow sparking gap between the electrode and workpiece. The narrow gap was the main problem for blocking the material removal from the machining zone and more debris concentration in the bottom of the electrode resulting in thickened heat affected zone formation. This narrow sparking gap affected the material removal mechanism of CFRP and it was a complex phenomenon in the macro-EDM and micro-EDM where sparking happened both at the end face and side surface of the square electrode resulting in more debris formed. The stage of the burning of the matrix and resin was varied due to variation in thermal properties resulting in unbalancing to removing material from the machining zone. This phenomenon was related to the amount of pulse duration, current, and duty cycle. An unbalancing effect of material removal of CFRP greatly affects the properties of the electrolyte. This was also the reason for forming debris in the

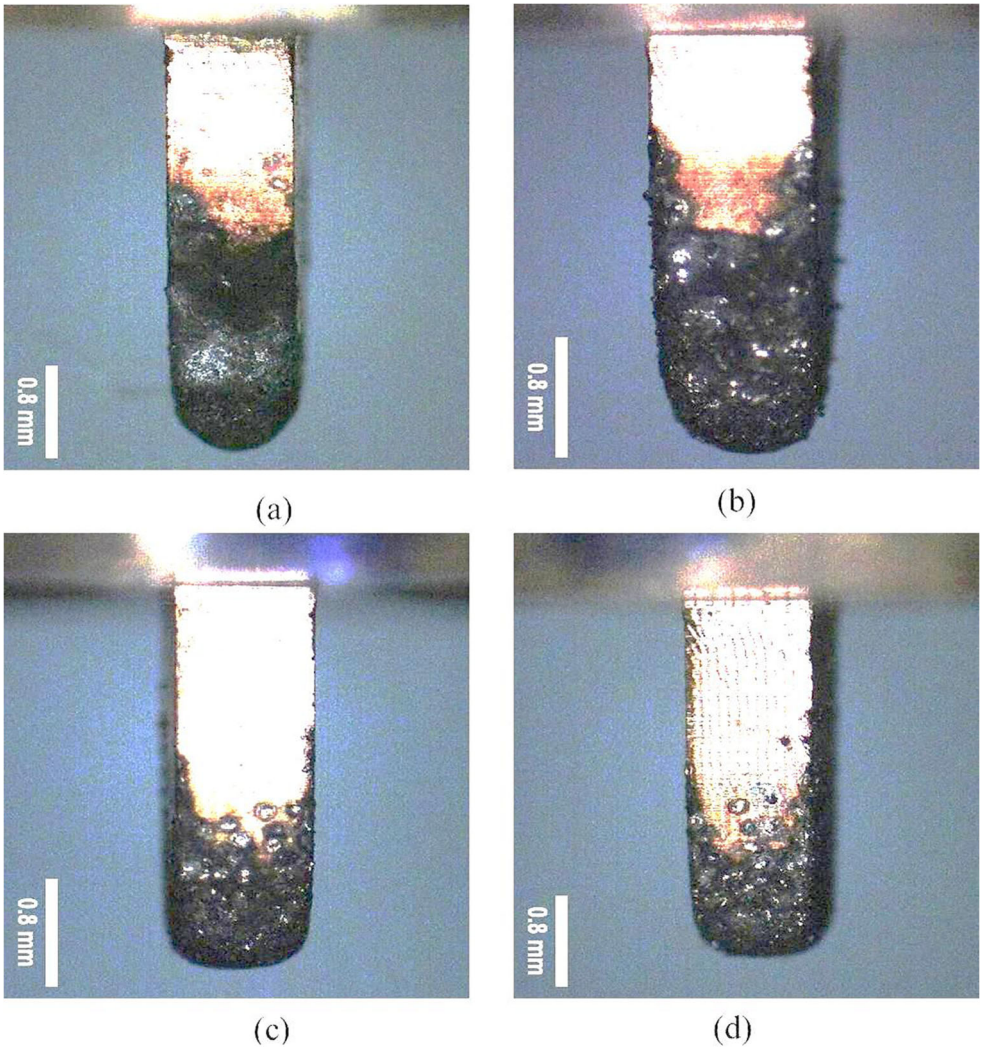

Fig. 8 Worn out electrode at bottom view: (a) 4st experiment, (b) 8th experiment, (c) 12th experiment, (d) 16 th experiment

machining zone. The selection of dielectric fluid pressure also greatly affects the electrical properties of dielectric fluid due to the contamination of electrolytes resulting in reducing the efficiency of material removal. In this work, the 0.7 kg/cm^2 kerosene dielectric pressure was selected for processing. It was found that the pressure value was inadequate for removing the debris from the machining zone resulting in debris clogs in the machining zone. Simultaneously, the spark was supplied without removing work material resulting in a thicken heat affected zone formed. On the other hand, SiC particles play an important role in the EDM process. The effects of the addition of SiC to dielectric fluid were reducing the insulating strength and increasing the sparking gap distance, resulting in a high material removal rate. Inversely, debris formation greatly affected the material removal rate. Hence, low dielectric fluid pressure was the main reason for the formation of debris and black products in the machined zone. The remaining process parameters were not much affecting the material removal rate and debris formation.

3.6 Modeling

The modeling was used to find the relation between the process parameters and responses. The regression equations were developed in the squareness, hole depth, and surface roughness using statistical software. The regression equations found that the sum of square value, R-square value, and R-square adjusted values were obtained in good-fit for further prediction.

$$\text{Squareness} = 0.996 + 0.0019 \text{ x Cp} + 0.0025 \text{ x Ton} - 0.00192 \text{ x DC} - 0.00045 \text{ x I}$$
$$S = 0.014, \text{R-Sq} = 93.3\%, \text{R-Sq (adj)} = 90.8\% \quad (10)$$

$$\text{Hole depth} = 0.0564 + 0.023 \text{ x Cp} + 0.00154 \text{ x Ton} - 0.00195 \text{ x DC} - 0.00277 \text{ x I}$$
$$S = 0.013, \text{R-Sq} = 98.8\%, \text{R-Sq (adj)} = 98.4\% \quad (11)$$

$$\text{Surface roughness} = 0.792 + 0.261 \text{ x Cp} + 0.0256 \text{ x Ton} + 0.0537 \text{ x DC} + 0.0178 \text{ x I}$$
$$S = 0.267, \text{R-Sq} = 96.9\%, \text{R-Sq (adj)} = 95.8\% \quad (12)$$

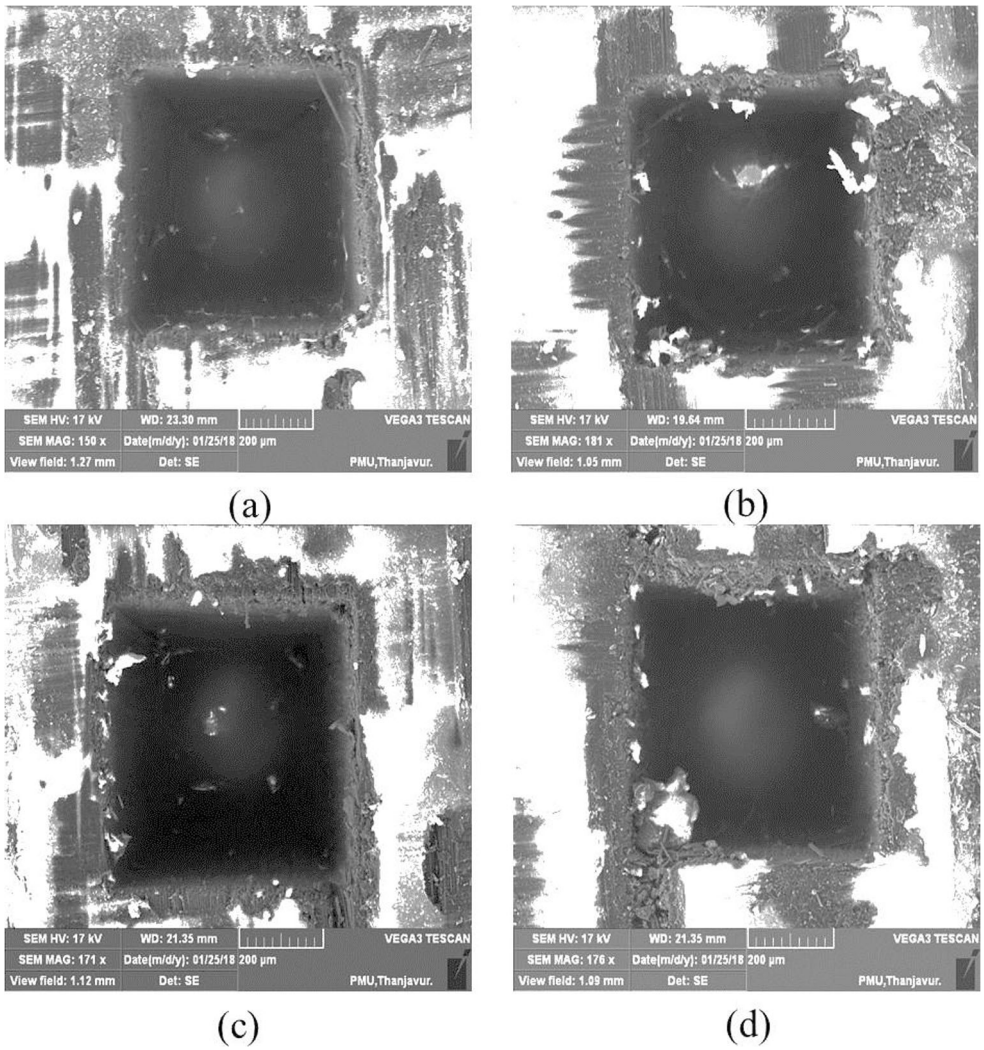

Fig. 9 Details of machined surface defects: (a) 4st experiment, (b) 8th experiment, (c) 12th experiment, (d) 16 th experiment

The unit of different responses and input parameters are given below.

Squareness (Sq. ness) = no unit.
Hole depth (HD) = mm.
Surface roughness (SR) = µm.
Concentration of SiC (Cp) = g/l.
Pulse duration (Ton) = µs.
Current (I) = amp.
Duty cycle (DC) = %.

The contribution percentages for squareness, hole depth, and surface roughness also formed, which is shown in Fig. 10. The variance analysis found that the pulse duration has a highly contributing percentage for improving the squareness of the hole. Similarly, the concentration of SiC has a highly contributing percentage for improving the surface roughness and hole depth. Table 6 shows the experimental data related to numerical results of squareness, hole depth, and surface roughness and found that percentage deviations are an acceptable limit.

3.7 Determination of Optimum Process Parameters

To determine the optimum parameters of multiple objectives, and the ARAS method was used. The ARAS calculating procedure is presented in Table 7. The surface roughness and squareness were considered lower, whereas the hole depth was considered as higher the better. In the ARAS method, the hole depth was considered beneficial criteria, whereas the surface roughness and squareness were considered non-beneficial criteria. The non-beneficial criteria were converted into beneficial criteria by inverting the non-beneficial criteria. The responses were formed as a decision matrix. The normalization of responses was calculated based on the response objectives. The hole depth was considered 0.4 weightage whereas surface roughness and squareness were considered 0.3 weightage. The weightage of responses was selected based on the industrial expert. The weighted normalization of responses for beneficial criteria was calculated. The optimality function and degree of utility were calculated for each alternative. The rank was calculated according to the degree of

Table 6 Experimental data related with numerical results of squareness, hole depth and surface roughness

S.No.	Actual experimmental data			Predicted by linear regression			Deviation in % between Actual vs linear regression		
	Sq. ness	HD	SR	Sq. ness	HD	SR	Sq. ness	HD	SR
1	1.044	0.177	1.941	1.038	0.164	2.309	0.548	7.339	−18.975
2	1.067	0.18	2.565	1.071	0.178	2.836	−0.379	1.294	−10.577
3	1.12	0.181	3.623	1.104	0.191	3.363	1.446	−5.707	7.168
4	1.132	0.197	3.652	1.137	0.205	3.890	−0.403	−4.056	−6.525
5	1.026	0.222	3.691	1.040	0.241	3.532	−1.388	−8.572	4.310
6	1.076	0.255	4.254	1.081	0.262	3.844	−0.435	−2.937	9.636
7	1.121	0.297	4.656	1.109	0.291	4.444	1.038	2.185	4.564
8	1.135	0.322	4.752	1.150	0.312	4.756	−1.304	3.115	−0.078
9	1.049	0.342	4.796	1.043	0.324	4.719	0.562	5.383	1.608
10	1.089	0.37	5.044	1.078	0.348	5.175	1.041	5.857	−2.591
11	1.145	0.394	5.374	1.128	0.389	5.201	1.521	1.353	3.221
12	1.158	0.405	5.836	1.162	0.413	5.657	−0.358	−2.077	3.072
13	1.031	0.409	5.846	1.049	0.423	5.799	−1.713	−3.367	0.802
14	1.099	0.446	6.005	1.091	0.455	6.040	0.737	−2.087	−0.585
15	1.147	0.466	6.094	1.130	0.466	6.424	1.522	0.067	−5.407
16	1.161	0.505	6.527	1.172	0.498	6.665	−0.929	1.341	−2.107

utility. The first experiment has been found as the best alternative process parameters based on the high optimality function and the first rank of the degree of utility. The best alternative process parameters for machining CFRPs were the concentration of SiC: 4 g/l, pulse duration: 15 µs, duty cycle: 1%, and current: 2 amp. The rank-based comparisons were carried out between the GRA, DFA, and proposed algorithm and it is shown in Table 8. The best alternative process parameters were verified through a confirmation test and it is shown in Table 9. The ARAS method has improved CFRP performance. In addition, the non-contact roughness measurement was used for measuring the cross-section of surface roughness of 0.8-mm blind micro square hole and roughness of 1.28 µm was achieved, which was better than the confirmation test roughness value.

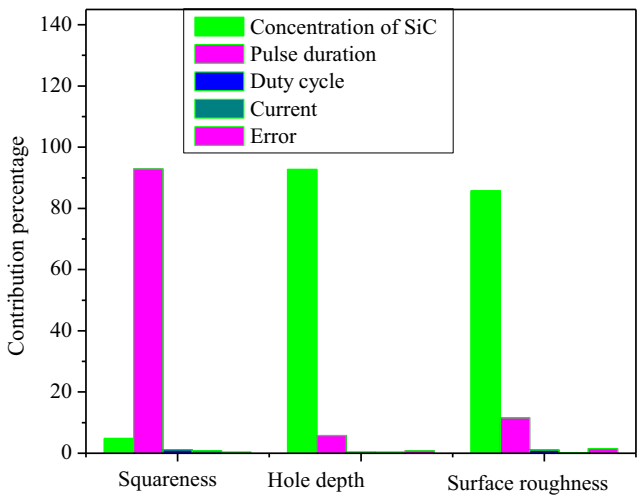

Fig. 10 Contribution percentage for responses

3.8 Comparison with Previous Studies

Comparative studies were conducted between the current study and published works, which are shown in Table 10. More works were focused to study the surface roughness and removal of burrs in the machined CFRP. No works were found that the effect of SiC concentration on squareness, hole depth, and surface roughness of CFRP was studied using EDM with the square copper electrode. The trail tests found that the through-hole was not obtained by increasing the above 16 g/l SiC due to the higher electrode wear observed. The squareness of the blind square hole of CFRP has not been studied using more researchers. More works were focusing on circular holes forming on CFRPs using EDM [7–11]. The hole depth was directly proportional to the current and pulse duration due to the heat energy. SiC powder mixed kerosene has improved the hole depth due to the increased thermal conductivity of the dielectric medium. The hole depth variation was observed between the previous study [8] and the current result due to the electrode thermal conductivity. Compared to the surface roughness of CFRP between the SiC powder mixed dielectric fluid [20, 22] and non-power mixed dielectric fluid performance [10, 11, 44], the SiC power mixed dielectric fluid produces better performance. The surface roughness of the current study was better than other studies [10, 11, 16, 17,

Table 7 Additive ratio assessment calculations

	Experimental results			Decision-making matrix			Normalized data			Weight normalized data			Si	Ki	Rank
Max or Min	Sq. ness	HD	SR	Sq. ness	HD	SR	Sq. ness	HD	SR	Sq. ness	HD	SR			
No.	1.026	0.505	1.941	0.975	0.505	0.515	0.063	0.089	0.119	0.019	0.036	0.036	0.090	1.000	
1	**1.044**	**0.177**	**1.941**	**0.958**	**0.177**	**0.515**	**0.062**	**0.031**	**0.119**	**0.018**	**0.012**	**0.036**	**0.067**	**0.740**	**1**
2	1.067	0.18	2.565	0.937	0.180	0.390	0.060	0.032	0.090	0.018	0.013	0.027	0.058	0.641	6
3	1.12	0.181	3.623	0.893	0.181	0.276	0.057	0.032	0.064	0.017	0.013	0.019	0.049	0.545	16
4	1.132	0.197	3.652	0.883	0.197	0.274	0.057	0.035	0.063	0.017	0.014	0.019	0.050	0.554	15
5	1.026	0.222	3.691	0.975	0.222	0.271	0.063	0.039	0.063	0.019	0.016	0.019	0.053	0.591	12
6	1.076	0.255	4.254	0.929	0.255	0.235	0.060	0.045	0.054	0.018	0.018	0.016	0.052	0.579	14
7	1.121	0.297	4.656	0.892	0.297	0.215	0.057	0.052	0.050	0.017	0.021	0.015	0.053	0.588	13
8	1.135	0.322	4.752	0.881	0.322	0.210	0.057	0.057	0.049	0.017	0.023	0.015	0.054	0.602	11
9	1.049	0.342	4.796	0.953	0.342	0.209	0.061	0.060	0.048	0.018	0.024	0.014	0.057	0.632	10
10	1.089	0.37	5.044	0.918	0.370	0.198	0.059	0.065	0.046	0.018	0.026	0.014	0.058	0.638	7
11	1.145	0.394	5.374	0.873	0.394	0.186	0.056	0.069	0.043	0.017	0.028	0.013	0.058	0.638	8
12	1.158	0.405	5.836	0.864	0.405	0.171	0.056	0.071	0.040	0.017	0.029	0.012	0.057	0.633	9
13	1.031	0.409	5.846	0.970	0.409	0.171	0.062	0.072	0.040	0.019	0.029	0.012	0.059	0.659	5
14	1.099	0.446	6.005	0.910	0.446	0.167	0.059	0.079	0.039	0.018	0.031	0.012	0.061	0.672	4
15	1.147	0.466	6.094	0.872	0.466	0.164	0.056	0.082	0.038	0.017	0.033	0.011	0.061	0.677	3
16	1.161	0.505	6.527	0.861	0.505	0.153	0.055	0.089	0.035	0.017	0.036	0.011	0.063	0.697	2

20, 22, 44] due to the addition of SiC to kerosene to provide better results. The better copper electrode wear was observed compared to previous results [7, 44] due to the electrode thermal conductivity.

Table 8 Rank comparison based on the GRA, DFA and proposed algorithm

S. No.	GRA [49]	DFA [50]	Proposed algorithm
1	1	1	1
2	2	2	6
3	4	5	16
4	5	7	15
5	3	3	12
6	7	4	14
7	9	8	13
8	11	11	11
9	8	6	10
10	10	9	7
11	13	12	8
12	14	15	9
13	6	10	5
14	12	13	4
15	15	14	3
16	16	16	2

4 Conclusions

A great effort is made to study the concentration of SiC powder and EDM parameters on squareness, hole depth, and surface roughness on square blind hole CFRP using EDM with the square copper electrode. The conclusions have the following as.

- The percentage of concentration of SiC and pulse duration greatly affect the squareness, hole depth, surface roughness, and electrode wear length.
- A corner radius has formed on the machined square holes due to the area effect and the skin effect.
- Low thermal heat energy has been used for producing the minimum surface roughness and minimum thermal damage.
- Deformed electrode wears were formed in all the CFRP machined corners due to unstable sparking produced.
- Cutting edge irregularity has formed in the machined edges.
- Regression models for EDMs are a good fit for prediction.
- ARAS method provides consistent results with other standard methods and improved the performance measures.

Acknowledgments The authors thank the COVAI EDM at Coimbatore for providing a machining facility. The authors are also thankful to Periyar Maniammai Institute of Science & Technology at Vallam for providing a scanning electron microscopy facility.

Table 9 Confirmation experiment

	Raw Data	Experiment
Conditions	Cp=4 g/l/ Ton=15 μs/ DC=1%/ I=1 amp	Cp=4 g/l/ Ton=15 μs/ DC=1%/ I=1 amp
Squareness (−)	1.044	1.015
Hole depth (mm)	0.177	0.234
Surface roughness (μm)	1.941	1.231
Ki	0.740	0.818
Improvement in Ki=0.078		

Contributions PV Arul Kumar: Conceptualization, Methodology, Writing Reviewing discussion and Editing. J. Vivek: computation, Methodology, Software, Writing discussion and N. Senniangiri: Conceptualization and analysis, Writing-review, writing the manuscript, Methodology, Software, and writing – discussion, S. Nagarajan: review manuscript language, B. Alshahrani: review manuscript language, K. Chandrasekaran: review manuscript language.

Funding The authors did not receive support from any organization for the submitted work.

Data Availability The available data and material had been used and discussed in the manuscript.

Declaration

Consent to Participate All persons named as authors in this manuscript have participated in the planning, design, and performance of the research and the interpretation of the results.

Consent for Publication All authors have endorsed the publication of this research.

Ethics Declarations The manuscript has not been published elsewhere and it has not been submitted simultaneously for publication elsewhere.

Declaration of Competing Interest The authors declare that they have no known competing financial interests or personal relationships that could have appeared to influence the work reported in this paper.

References

1. Samal P, Babu DM, Kiran SV, Surekha B, Vundavilli PR, Mandal A (2020). Study of microstructural and machining characteristics of hypereutectic Al-Si alloys using wire-EDM for photovoltaic application. Silicon, pp.1–13
2. Phan NH, Muthuramalingam T (2020) Multi criteria decision making of vibration assisted EDM process parameters on machining silicon steel using Taguchi-DEAR methodology. Silicon, pp.1-7
3. Muthuramalingam T, Saravanakumar D, Babu LG, Phan NH, Pi VN (2019) Experimental investigation of white layer thickness on EDM processed silicon steel using ANFIS approach. Silicon, pp.1-7

Table 10 Comparison of present results with published literatures

R.No.	Materials/ Additives	Dielectric medium	Electrode Material/size	Cp (g/l)	Ton (μs)	DC (%)	I (amp)	Sq. ness	Hole depth (mm)	SR (μm)	Tool Wear (mm)
[7]	CFRP/−	Oil	WC / 0.3 mm	–	50	–	–	–	0.2	8	0.025
[8]	CFRP/−	EDM oil	WC/0.110 mm	–	–	–	–	–	1.2	–	–
[9]	CFRP/−	–	Cu/0.5	–	–	–	–	–	0.25	–	–
[10]	CFRP/−	Esso mentor	Cu/10 mm	–	25–160	–	1–4	–	–	15–45	–
[11]	CFRC/−	Castrol	Cu/4.42 mm	–	200	–	1.5	–	–	5.14	–
[16]	CFRP/−	kerosene	Gr/ 1 mm	–	100	–	5	–	–	4.8	–
[17]	CFRP/−	EDM oil	Cu/2 mm	–	70	–	2	–	–	4	–
[20]	Die steel/SiC	EDM oil	Cu/square	6	150	90	3	–	–	3	–
[21]	Titanium/SiC	EDM oil	Cu/42 mm	25	2–20	80	0.1, 1	–	2.6 mm^3/min	–	–
[22]	Titanium/SiC	–	–	5–20	25	–	–	–	–	6.77	–
[34]	CFRP/−	Kerosene	Cu/8 mm	–	50	–	–	–	–	7	1.2 g/min
Current experimental results											
Present work	CFRP/SiC	kerosene	Cu/0.8 mm square electrode	4	15	1	2	1.015	0.234	1.231	0.31–1.168

4. Ramanujam N, Dhanabalan S, Raj Kumar D, Jeyaprakash N (2021) "Investigation of micro-hole quality in drilled CFRP laminates through CO2 laser." Arab J Sci Eng 1–19
5. Raj Kumar D, Jeyaprakash N, Yang C, Sivasankaran S (2020) "Optimization of drilling process on carbon-fiber reinforced plastics using genetic algorithm." Surface Review and Letters 2050056
6. Raj Kumar D, Jeyaprakash N, Yang C-H, Ramkumar KR (2020) Investigation on drilling behavior of CFRP composites using optimization technique. Arab J Sci Eng 45:8999–9014
7. Teicher U, Müller S, Münzner J, Nestler A (2013) Micro-EDM of carbon fibre-reinforced plastics. Procedia Cirp 6:320–325
8. Kumar R, Agrawal PK, Singh I (2018) Fabrication of micro holes in CFRP laminates using EDM. J Manuf Process 31:859–866
9. Park SH, Kim G, Lee W, Min BK, Lee SW and Kim TG (2015). Microhole machining on precision CFRP components using electrical discharging machining. In 20th international conference on composite materials, Copenhagen, Denmark
10. Lau WS, Wang M, Lee WB (1990) Electrical discharge machining of carbon fibre composite materials. Int J Mach Tools Manuf 30(2): 297–308
11. Gourgouletis K, Vaxevanidis NM, Galanis NI, Manolakos DE (2011) Electrical discharge drilling of carbon fibre reinforced composite materials. Int J Mach Mach Mater 10(3):187–201
12. George PM, Raghunath BK, Manocha LM, Warrier AM (2004) EDM machining of carbon–carbon composite—a Taguchi approach. J Mater Process Technol 145(1):66–71
13. Kurniawan R, Kumaran ST, Prabu VA, Zhen Y, Park KM, Kwak YI, Islam MM, Ko TJ (2017) Measurement of burr removal rate and analysis of machining parameters in ultrasonic assisted dry EDM (US-EDM) for deburring drilled holes in CFRP composite. Measurement 110:98–115
14. Islam MM, Li CP, Won SJ, Ko TJ (2017) A deburring strategy in drilled hole of CFRP composites using EDM process. J Alloys Compd 703:477–485
15. Mazarbhuiya RM, Dutta H, Debnath K, Rahang M (2020) Surface modification of CFRP composite using reverse-EDM method. Surfaces and Interfaces 18:100457
16. Guu YH, Hocheng H, Tai NH, Liu SY (2001) Effect of electrical discharge machining on the characteristics of carbon fiber reinforced carbon composites. J Mater Sci 36(8):2037–2043
17. Lodhi BK, Verma D, Shukla R (2014) Optimization of machining parameters in EDM of CFRP composite using Taguchi technique. Int J Mech Eng Technol 5(10):70–77
18. Niamat M, Sarfraz S, Aziz H, Jahanzaib M, Shehab E, Ahmad W, Hussain S (2017) Effect of different dielectrics on material removal rate, electrode wear rate and microstructures in EDM. Procedia Cirp 60:2–7
19. Das S, Paul S, Doloi B (2020) Feasibility assessment of some alternative dielectric mediums for sustainable electrical discharge machining: a review work. J Braz Soc Mech Sci Eng 42(4):1–21
20. Tripathy S, Tripathy DK (2017) Surface characterization and multi-response optimization of EDM process parameters using powder mixed dielectric. Materials Today: Proceedings 4(2):2058–2067
21. Chow HM, Yang LD, Lin CT, Chen YF (2008) The use of SiC powder in water as dielectric for micro-slit EDM machining. J Mater Process Technol 195(1–3):160–170
22. Öpöz TT, Yaşar H, Ekmekci N, Ekmekci B (2018) Particle migration and surface modification on Ti6Al4V in SiC powder mixed electrical discharge machining. J Manuf Process 31:744–758
23. Chow HM, Yan BH, Huang FY, Hung JC (2000) Study of added powder in kerosene for the micro-slit machining of titanium alloy using electro-discharge machining. J Mater Process Technol 101(1–3):95–103
24. Jung JH, Kwon WT (2010) Optimization of EDM process for multiple performance characteristics using Taguchi method and Grey relational analysis. J Mech Sci Technol 24(5):1083–1090
25. Chen ST, Yeh MC (2016) Development of an in-situ high-precision micro-hole finishing technique. J Mater Process Technol 229:253–264
26. Liu Q, Zhang Q, Zhu G, Wang K, Zhang J, Liu Q et al (2016) Effect of electrode size on the performances of micro-EDM. Mater Manuf Process 31:391–396
27. Al-Ahmari AMA, Rasheed MS, Mohammed MK, Saleh T (2016) A hybrid machining process combining micro-EDM and laser beam machining of nickel – titanium-based shape memory alloy. Mater Manuf Process 31:447–455
28. Kumar H, Davim JP (2011)) Role of powder in the machining of Al-10% SiCp metal matrix composites by powder mixed electric discharge machining. J Compos Mater 45(2):133–151
29. Mohri N, Saito N, Higashi M (1991) A new process of finish machining on free surface by EDM methods. Annals of CIRP 40(1): 207210
30. Vishwakarma UK, Dvivedi A, Kumar P (2014) Comparative study of powder mixed EDM and rotary tool EDM performance during machining of Al-SiC metal matrix composites. Int J Mach Mach Mater 16(2):113–128
31. Islam MM, Li CP, Ko TJ (2017) Dry electrical discharge machining for deburring drilled holes in CFRP composite. International Journal of Precision Engineering and Manufacturing-Green Technology 4(2):149–154. https://doi.org/10.1007/s40684-017-0018-x
32. Isbilir O, Ghassemieh E (2013) Comparative study of tool life and hole quality in drilling of CFRP/titanium stack using coated carbide drill. Mach Sci Technol 17:380–409
33. Elsiti, N.M. and Noordin, M.Y., 2017. Experimental investigations into the effect of process parameters and Nano-powder (Fe2O3) on material removal rate during micro-EDM of co-Cr-Mo. In key engineering materials (Vol. 740, pp. 125-132). Trans tech publications ltd.
34. Debnath K, Dutta H, Sarma DK (2021). Influence of different tool materials on the machining performance in μED-milling of CFRP composites. In machining and machinability of Fiber reinforced polymer composites (pp. 207-224). Springer, Singapore
35. Abdallah R, Soo SL, Hood R (2021) The influence of cut direction and process parameters in wire electrical discharge machining of carbon fibre–reinforced plastic composites. Int J Adv Manuf Technol 113(5):1699–1716
36. Devi, L., Paswan, K., Chattopadhyaya, S. and Pramanik, A., 2021. Influence of low-frequency vibration in die sinking EDM: a review. In IOP conference series: materials science and engineering (Vol. 1104, no. 1, p. 012010). IOP publishing
37. Dutta H, Debnath K, Sarma DK (2021) Improving the micro-electrical-discharge drilling performance of carbon fibre-reinforced polymer: role of assisting-electrode and shaped tool. Int J Mach Mach Mater 23(2):191–207
38. Hashizu M, Hayakawa S, Itoigawa F (2020) Influence of short-circuitng on machined surface quality in electrical discharge machining of carbon fiber reinforced plastics. Procedia CIRP 95: 403–407
39. Kumaran VU, Kliuev M, Billeter R, Wegener K (2020) Influence of carbon based fillers on EDM machinability of CFRP. Procedia CIRP 95:437–442
40. Dutta H, Debnath K, Sarma DK (2020) Multi-objective optimization of hole dilation at inlet and outlet during machining of CFRP by μEDM using assisting-electrode and rotating tool. Int J Adv Manuf Technol 110(9):2305–2322
41. Makudapathy C, Sundaram M (2020) High aspect ratio machining of carbon Fiber reinforced plastics by electrical discharge machining process. Journal of Micro and Nano-Manufacturing
42. Dutta H, Debnath K, Sarma DK (2021). Investigation on cutting of thin carbon fiber-reinforced polymer composite plate using sandwich electrode-assisted wire electrical-discharge machining.

Proceedings of the institution of mechanical engineers, part E: journal of process mechanical engineering, p.09544089211013318
43. Wu C, Cao S, Zhao YJ, Qi H, Liu X, Liu G, Guo J, Li HN (2021) Preheating assisted wire EDM of semi-conductive CFRPs: principle and anisotropy. J Mater Process Technol 288:116915
44. Selvakumar G, Sarkar S, Mitra S (2012) Experimental investigation on die corner accuracy for wire electrical discharge machining of Monel 400 alloy. Proceedings of the Institution of Mechanical Engineers, Part B: Journal of Engineering Manufacture 226(10): 1694–1704
45. Balamurugan K, Uthayakumar M, Ramakrishna M, Pillai UTS (2020) Air jet Erosion studies on mg/SiC composite. Silicon 12(2):413–423
46. Chinnamahammad Bhasha A, Balamurugan K (2020) Studies on Al6061 nanohybrid composites reinforced with SiO 2/3x% of TiC-a agro-waste. Silicon, pp.1-14
47. Garikapati P, Balamurugan K, Latchoumi TP and Malkapuram R (2020). A cluster-profile comparative study on machining AlSi 7/63% of SiC hybrid composite using agglomerative hierarchical clustering and K-means. Silicon, pp1–12
48. Balamurugan K, Uthayakumar M, Sankar S, Hareesh US, Warrier KGK (2020) Process optimisation and exhibiting correlation in the exploitable variable of AWJM. Int J Mater Prod Technol 61(1):16–33
49. Balamurugan K, Uthayakumar M, Sankar S, Hareesh US, Warrier KGK (2017) Mathematical modelling on multiple variables in machining LaPO4/Y2O3 composite by abrasive water jet. Int J Mach Mach Mater 19(5):426–439
50. Antil P, Kumar Antil S, Prakash C, Królczyk G, Pruncu C (2020). Multi-objective optimization of drilling parameters for orthopaedic implants. Measurement and Control, p.0020294020947126
51. Kharb SS, Antil P, Singh S, Antil SK, Sihag P, Kumar A (2020) Machine learning-based Erosion behavior of silicon carbide reinforced polymer composites. Silicon. 13:1113–1119. https://doi.org/10.1007/s12633-020-00497-z
52. Antil SK, Antil P, Singh S, Kumar A, Pruncu CI (2020) Artificial neural network and response surface methodology based analysis on solid particle Erosion behavior of polymer matrix composites. Materials 13(6):1381
53. Bachchan AA, Das PP, Chaudhary V (2021) Effect of moisture absorption on the properties of natural fiber reinforced polymer composites: a review. Materials Today: Proceedings
54. Bañon F, Sambruno A, González-Rovira L, Vazquez-Martinez JM, Salguero J (2021) A review on the abrasive water-jet machining of metal–carbon fiber hybrid materials. Metals 11(1):164
55. Prasad KS, Chaitanya G (2021). Optimization of process parameters on surface roughness during drilling of GFRP composites using taguchi technique. Materials today: proceedings, 39, pp.1553-1558
56. Kumaran ST, Ko TJ, Uthayakumar M, Islam MM (2017) Prediction of surface roughness in sabrasive water jet machining of CFRP composites using regression analysis. J Alloys Compd 724:1037–1045
57. Kumaran ST, Ko TJ, Kurniawan R, Li C, Uthayakumar M (2017) ANFIS modeling of surface roughness in abrasive waterjet machining of carbon fiber reinforced plastics. J Mech Sci Technol 31(8): 3949–3954
58. Thakur RK, Singh KK, Ramkumar J (2021) Impact of nanoclay filler reinforcement on CFRP composite performance during abrasive water jet machining. Materials and Manufacturing Processes, pp:1–10
59. Dahooie JH, Zavadskas EK, Abolhasani M, Vanaki A, Turskis Z (2018) A novel approach for evaluation of projects using an interval–valued fuzzy additive ratio assessment (ARAS) method: a case study of oil and gas well drilling projects. Symmetry 10(2):45
60. Dhanabalan S, Sivakumar K, Narayanan CS (2013) Optimization of machining parameters of EDM while machining Inconel 718 for form tolerance and orientation tolerance
61. Dhanabalan S, Sivakumar K, Sathiya Narayanan C (2014) Analysis of form tolerances in electrical discharge machining process for Inconel 718 and 625. Mater Manuf Process 29(3):253–259
62. Yadav RN (2019) Electro-chemical spark machining–based hybrid machining processes: research trends and opportunities. Proc Inst Mech Eng B J Eng Manuf 233(4):1037–1061
63. Jafferson JM, Hariharan P, Ram Kumar J (2014) Effects of ultrasonic vibration and magnetic field in micro-EDM milling of non-magnetic material. Mater Manuf Process 29(3):357–363
64. Jeyaprakash N, Yang CH, Raj Kumar D (2020) Machinability study on CFRP composite using Taguchi based grey relational analysis. Materials Today: Proceedings 21(3):1425–1431
65. Rajkumar D, Ranjithkumar P and Narayanan CS (2017) Optimization of machining parameters on microdrilling of CFRP composites by Taguchi based desirability function analysis